Chemical Engineering Journal 151 (2009) 160–167

Contents lists available at ScienceDirect

Chemical Engineering Journal

journal homepage: www.elsevier.com/locate/cej

Effect of gas–liquid flow pattern on air-sparged cross-flow microfiltration of yeast suspension

Kuo-Jen Hwang*, Chin-En Hsu

Department of Chemical and Materials Engineering, Tamkang University, 151 Ying-Chuan Rd., Tamsui, Taipei Hsien 25137, Taiwan

ARTICLE INFO

Article history:
Received 28 February 2008
Received in revised form 9 July 2008
Accepted 10 February 2009

Keywords:
Cross-flow microfiltration
Air-sparging
Cake properties
Gas–liquid flow pattern
Bio-separation

ABSTRACT

Effect of gas–liquid flow pattern on the performance of air-sparged cross-flow microfiltration of yeast suspension is studied. The pseudo-steady filtration flux and the cake properties under various operating conditions are measured and discussed. The shear stress acting on the membrane surface and the critical condition for particle deposition are analyzed theoretically based on hydrodynamic models. The cake mass is markedly reduced by increasing the wall shear stress. However, the average specific cake filtration resistance increases with increasing the wall shear stress due to more compact cake structure. The increase in the average specific filtration resistance of cake due to air-sparging is more significant in bubbly flows. Consequently, the filtration flux will be increased by air-sparging due to the cake reduction in slug flow microfiltration. However, a contrary result is obtained for bubbly flows due to the drastic increase in the average specific filtration resistance of cake. Therefore, a microfiltration operating under slug flow is more effective to enhance the filtration flux by air-sparging. In addition, the proposed model provides a method to quantitatively relate the filtration flux to operating parameters. The relationships are also strongly dependent on the gas–liquid flow pattern.

1. Introduction

Cross-flow microfiltration is an efficient method for separating microbial cells or bio-mixtures in biochemical processes. Although it has been widely used, the flux decline due to membrane fouling is still a major obstacle to keep on a high performance during operation. In order to improve filtration flux or membrane selectivity, the effectiveness of sparging air-bubbles into the filter channel has been studied [1–6]. The flux was correlated with operating variables in some empirical equations [5,6]; however, the coefficients should be determined by routine experiments.

Since the shear stress acting on the membrane surface can be increased by sparging air-bubbles into the filter channel, this method may effectively reduce cake mass and enhance filtration flux in most conditions [1–6]. However, the magnitude of wall shear stress is not only dependent on the fluid velocities but also on the gas–liquid flow pattern. A bubbly flow occurs under low gas volumetric fraction, and it changes to a slug flow when the gas faction exceeds a critical value. For a bio-reaction process, the existence of small bubbles in bubbly flow is appropriate for supplying more gas–liquid interface area for improving oxygen transfer. However, a slug flow generates higher tangential shear stress on the membrane surface in cross-flow filtration, which may be more effective for limiting particle deposition or membrane fouling. Therefore, to understand the filtration performances in cross-flow microfiltration under different gas–liquid flow patterns has benefits in the development of future biotechnology.

Cui and Wright [1,2] studied the effectiveness of gas sparging in up- and downward vertical filter tubes. They found that the flux could be enhanced as high as 60- to 320-fold in air-sparging ultrafiltration of dextran, blue dextran or BSA suspensions. Mercier-Bonin and Fonade [4] carried out the cross-flow microfiltration of enzyme/yeast mixtures. The filtration flux was improved 140% in a gas–liquid slug flow; however, the enzyme transmission was drastically decreased under the same flow condition. In contrast, they also found that the flux and enzyme transmission were both slightly enhanced with a bubbly flow pattern.

Air-sparging in another filtration module configuration, hollow fiber membranes, was also studied in the past 20 years. Lee et al. [7] obtained a 100% flux enhancement in cross-flow ultrafiltration of *E. coli* under slug flow pattern. Cabassud et al. [8] analyzed the influence of hydrodynamic parameters of gas–liquid flow on the cake characteristics in ultrafiltration hollow fibers. They claimed that the flux enhancement was controlled by the mixing or turbulence near the membrane surface, and the cake structure seemed to be linked to mixing or the flow intermittence. Fane and his co-workers [9–11] discussed the effects of the arrangements of hollow fibers, bubble size, bubble frequency and the ratio of liquid to gas flow rate on the performance of

* Corresponding author. Tel.: +886 2 26215656x2614; fax: +886 2 26209887.
E-mail address: kjhwang@mail.tku.edu.tw (K.-J. Hwang).

1385-8947/$ – see front matter © 2009 Elsevier B.V. All rights reserved.
doi:10.1016/j.cej.2009.02.009

Nomenclature

A	cross-sectional area of the filter channel [m^2]
C_1	correction factor defined in Eq. (9)
C_2	correction factor defined in Eq. (10)
C_3	correction factor defined in Eq. (13)
C_4–C_5	coefficients defined in Eq. (16)
C_6	correction factor defined in Eq. (17)
Ca	capillary number defined by Eq. (7)
d_p	diameter of particles [m]
F_i	net interparticle force [N]
F_l	inertial lift force [N]
F_n	drag force exerted on particles in the filtration direction [N]
F_t	drag force exerted on particles in the suspension flow direction [N]
f_c	friction coefficient between particles
H	the clearance of the filter channel [m]
P	hydraulic pressure [N/m^2]
ΔP	filtration pressure [N/m^2]
Q	volumetric flow rate [m^3/s]
q_s	pseudo-steady state filtration flux [m^3/m^2 s]
R_c	resistance of the filter cake [m^{-1}]
R_t	overall filtration resistance [m^{-1}]
u	superficial velocity [m/s]
u_{pl}	lift velocity [m/s]
v	true velocity [m/s]
v_b	bubble velocity [m/s]
w_c	mass of dry cake per unit area [kg/m^2]
x	distance from the inlet of filter channel in suspension flow direction [m]

Greek letters

α_{av}	average specific filtration resistance of cake [m/kg]
β	rate of intermittency
δ	liquid film thickness [m]
γ	surface tension [N/m]
λ	void fraction in gas–liquid two-phase flow
μ	viscosity [kg/s m]
θ	gas injection factor defined in Eq. (1)
ρ	density [kg/m^3]
τ_w	shear stress acting on the membrane surface [N/m^2]

Subscripts

G	gas
L	liquid

cross-flow filtration of yeast or of bentonite suspensions. They indicated that increasing shear stress or generating vortices was an efficient way to enhance filtration flux. The membrane fouling could be reduced more effectively by sparging air-bubbles if the fiber axis was parallel to the fluid flow direction in outside-in ultrafiltration.

In this study, the shear stress acting on the membrane surface and the critical condition for particle deposition in a horizontal two-parallel-plate microfilter are analyzed theoretically based on hydrodynamic models. Effects of operating conditions, such as the flow rates of suspension and air-bubbles and the filtration pressure, on the filtration flux and cake properties are measured and discussed. The dependences of filtration flux or cake properties on the wall shear stress under different gas–liquid flow patterns are also derived.

2. Theory

2.1. Shear stress acting on the membrane surface

Fig. 1 is a schematic diagram of gas–liquid flow patterns in a horizontal cross-flow microfilter. The suspension flows from the left-hand side into the two-parallel-plate microfilter, the filtrate permeates downward through the porous bottom plate, while the concentrate flows out from the right-hand side. In general, the flow pattern of a gas–liquid two-phase flow can be related to the injection factor defined as [8]:

$$\theta \equiv \frac{u_G}{u_G + u_L} \tag{1}$$

where u_G and u_L are the superficial velocities of gas and liquid, respectively. The flow is bubbly when $\theta < 0.2$, small air bubbles disperse in the liquid in such a condition. When $0.2 < \theta < 0.9$, the formed large bubbles result in a slug flow. In the condition of high gas flow rate, e.g. $\theta > 0.9$, an annular flow occurs. Air occupies most core region in the channel, and liquid flows in the film near the channel walls. Referring to the system shown in Fig. 1, some particles are carried by the liquid to arrive at the membrane surface. A key factor to affect the stability of particles on the membrane surface is the shear stress produced by the tangential suspension flow. Therefore, to understand how the wall shear stress affected by operating conditions or gas–liquid flow pattern is the main gate to grasp filtration performance.

The wall shear stress is strongly dependent on the gas–liquid flow pattern. In recent year, Hwang and Wu [12] employed a liquid–gas two-phase flow model to calculate the pressure drop in the filter channel. The shear stress acting the membrane surface can then be estimated by a momentum balance on the filter channel, that is

$$\tau_w = \frac{H}{2}\left(-\frac{dP}{dx}\right) \tag{2}$$

where H is the channel clearance. This model can be used for bubbly flow in which the shear stress is increased by increasing both gas and liquid velocities. The true velocities of gas and liquid flows can be calculated, respectively, by the void fraction, λ [13]:

$$v_G = \frac{Q_G}{\lambda A}, \qquad v_L = \frac{Q_L}{(1-\lambda)A} \tag{3}$$

where A is the cross-sectional area of the flow channel, and Q_g and Q_l are the volumetric flow rates of gas and liquid, respectively.

In the slug flow regime, large flattened air bubbles flows across the filter channel as a plug-flow manner. The shear stress is therefore not uniform as the simple model described previously. In other words, the flow becomes intermittent and the wall shear stress can be calculated by summing the stresses produced in the liquid film around the gas bubbles, τ_{wG}, and in the liquid slugs, τ_{wL}, as below [14]:

$$\tau_w = \beta\tau_{wG} + \left(1-\beta\right)\tau_{wL} \tag{4}$$

where β is the rate of intermittency which is directly linked to the lengths of the long bubble and liquid slug. Since only a single-phase exists in the liquid slug, the shear stress of τ_{wL} can be estimated by the two-phase flow model proposed in the authors' previous study [12] once the true velocity of liquid is calculated using Eq. (3). On the other hand, the shear stress of τ_{wG} is mainly due to the velocity gradient in the liquid film exists between air-bubbles and the channel wall (or the membrane surface). Briceño and Joseph [15] derived a relation between the wall shear stress and the liquid film thickness in a horizontal

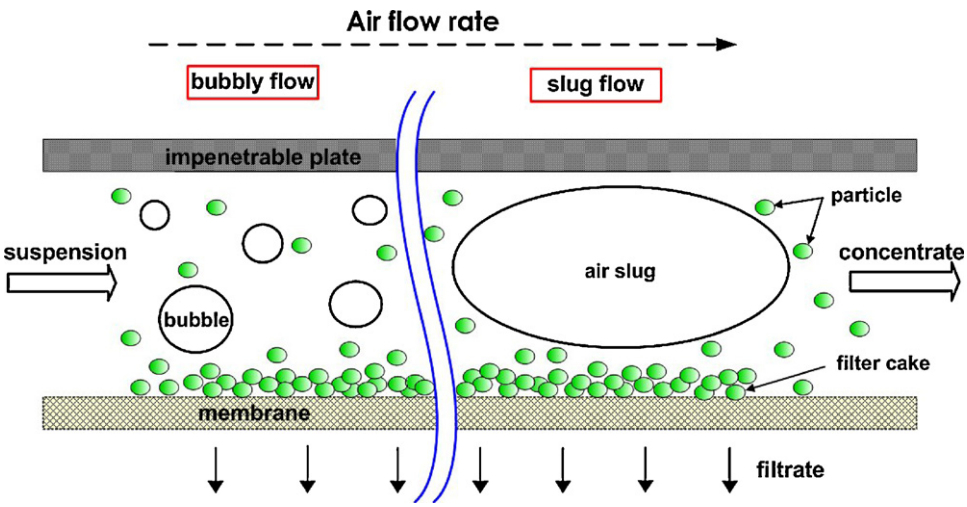

Fig. 1. The gas–liquid flow patterns in a cross-flow microfilter.

conduit as

$$\tau_{wG} = \mu_L \frac{u_L}{\delta} \tag{5}$$

where μ_L is the liquid viscosity and δ is the film thickness.

In the past, Bretherton [16] studied on the motion of a long gas bubble in a circular capillary filled with a liquid. Assuming that the gravity is negligible and no tangential stress acts at the gas–liquid interface, he claimed that the liquid film thickness is dependent on the tube radius, the liquid viscosity, the surface tension and the bubble velocity. According to his analysis, the film thickness can be estimated as follows [16]:

$$\delta = 1.337 \left(\frac{H}{2}\right) Ca^{2/3} \tag{6}$$

where Ca is the Capillary number and is defined as

$$Ca \equiv \frac{\mu_L v_b}{\gamma} \tag{7}$$

in which v_b is the bubble velocity and γ is the surface tension. The predictions of Eq. (6) have well agreement with the measurement in the conditions of Ca between 10^{-5} and 10^{-2} [16]. Therefore, the wall shear stress in a gas–liquid slug flow can be evaluated by Eq. (4).

2.2. Force balance model for particle deposition

According to the authors' previous studies, whether a particle staying on the membrane surface can deposit stably or not is determined by the external forces exerted on it [12,17,18]. Since the net gravity is negligible small compared to the other forces in most microfiltration, the force balance model at the pseudo-steady condition can be expressed as [17,18]:

$$F_t = f_c (F_n + F_l + F_i) \tag{8}$$

where f_c is the friction coefficient between particles, and F_t and F_n are the drag forces in the tangential (the suspension flow) and filtration directions, respectively, F_l is the inertial lift force and F_i is the net interparticle force. According to Eq. (8), the particle can deposit stably if the tangential force, the term on the left-hand side, is smaller than the net friction force, the term on the right-hand side. Otherwise, the particle will be swept away from the membrane surface.

The tangential drag force was analyzed by Hwang and Lin [18] and can be estimated by the modified Stokes law:

$$F_t = C_1 d_p^2 \tau_w \tag{9}$$

where d_p is the particle diameter, and C_1 is a correction factor for the existences of the filter cake and the membrane. It is evidence that the tangential force is proportional to the shear stress acting on the membrane surface for a given particle size.

Similar to the derivation in the tangential direction, the drag force in the filtration direction can be calculated by the following equation [18]:

$$F_n = 3\pi \mu_L d_p q_s C_2 \tag{10}$$

where q_s is the pseudo-steady filtration flux. The correction factor, C_2, can be given from the results of Goren [19]:

$$C_2 = \left(\frac{R_t d_p}{3} + 1.07^2\right)^{1/2} \tag{11}$$

where R_t is the overall filtration resistance including the resistances due to filter cake and membrane. However, the filtration resistance due to cake formation is much higher than that due to clean membrane in most conditions. Thus,

$$R_t \approx R_c = w_c \alpha_{av} \tag{12}$$

in which w_c and α_{av} are the mass and average specific filtration resistance of cake, respectively. Since the value of $R_t \times d_p$ in Eq. (11) is always much larger than 1.07^2, Eq. (10) can be simplified as

$$F_n = C_3 \mu_L d_p^{1.5} q_s R_c^{0.5} \tag{13}$$

In the region near the membrane surface, the velocity profile of liquid in the tangential direction can be simplified as linear. Therefore, the inertial lift velocity of a particle can be expressed as [20]:

$$u_{pl} = \frac{0.036 \rho_L d_p^3 \tau_w^2}{\mu_L^3} \tag{14}$$

Hence, the inertial lift force is significant only for large particles or under high wall shear stress. The drag force and inertial lift force in the filtration direction can then be summed up and expressed as

$$F_n + F_l = C_3 \mu_L d_p^{1.5} (q_s - u_{pl}) R_c^{0.5} \tag{15}$$

The negative sign in Eq. (15) is due to the opposite directions of these forces.

The interparticle forces caused by van der Waals force and electrostatic force for micron particles (yeast cells used in this study) are relatively small; therefore, the net interparticle force is assumed to be constant under a fixed suspension property in this model for simplicity. Substituting Eqs. (9) and (15) into Eq. (8), the force balance equation for a uniform particle size distribution can be rewritten as

$$\tau_w = C_4\mu_L(q_s - u_{pl})R_c^{0.5} + C_5 \quad (16)$$

or be rearranged to the form:

$$q_s = C_6\frac{\tau_w - C_5}{\mu_L R_c^{0.5}} + u_{pl} \quad (17)$$

Therefore, the relationship among the pseudo-steady filtration flux, the wall shear stress and the overall filtration resistance can be explained by Eq. (16) or (17).

3. Materials and methods

Yeast cells (*Saccharomyces cerevisiae*) purchased by ICN Biomedicals Inc. in Germany were suspended in de-ionized water for de-activity at 80 °C for 20 min. Yeast cells were then added into a 10 mM buffer solution mixed by sodium phosphate (Na_2HPO_4) and sodium hypophosphite (NaH_2PO_4) to prepare 0.2 wt% suspensions used in experiments. The density of yeast cells was measured as 1140 kg/m^3 after previous pretreatment, while the size of yeast cells ranged from 0.7 to 18 μm with a mean diameter of 4.7 μm. The filter membrane, made of mixed cellulose ester, was manufactured by ADVANTEC Co. in Japan. Its mean pore size and zeta potential were 0.1 μm and −24 mV, respectively. The clean membrane resistance under 100 kPa was measured as 2.97×10^{11} m^{-1}.

A schematic diagram of the cross-flow microfiltration system is shown in Fig. 2. The two-parallel-plate microfilter has a clearance of 2.0×10^{-3} m, a width of 2.0×10^{-2} m, and a length of 5.5×10^{-2} m. Cross-flow microfiltration experiments were carried out under various bulk suspension velocities, air volumetric flow rates and filtration pressures. The temperature of suspension was kept at 20 °C by a thermostat, while the suspension pH was kept at 7.0 during filtration. The suspension was pumped into the filter by a peristaltic pump (Watson-Marlow-Bredel Pumps, 500 Series, made in England). The flow rates of suspension and sparged-air were adjusted and measured by rotameters A and B, respectively. The filtration pressure was adjusted to setting value by the needle valve and indicated by the pressure gauges. The filtrate was collected into a receiver and was weighed by a load cell. The data were transferred to a personal computer for further calculation. The same amount of make-up water as the filtrate was duly added into the suspension tank to keep a constant suspension concentration during filtration. The flow pattern of the air-bubbles in the filter channel was observed and recorded by a video camera. The values of injection factor and void fraction within the conditions of this study are summarized in Table 1. Since the flow pattern is bubbly when $\theta < 0.2$ while is slug when $0.2 < \theta < 0.9$, it can be known that the gas–liquid flow patterns included both bubbly and slug flows. When the experiment was terminated, the cake formed on the filter membrane was sent to analyze its dry mass by an *ORION* moisture titrator [21] or observe its packing structure by SEM after quenching using liquid nitrogen.

Table 1
The values of injection factor and void fraction under various conditions.

u_L (m/s)	u_G (m/s)	θ	λ
0.1	0.02	0.167	0.087
	0.04	0.286	0.153
	0.08	0.444	0.245
0.3	0.02	0.063	0.031
	0.04	0.118	0.062
	0.08	0.211	0.116
0.5	0.02	0.039	0.017
	0.04	0.074	0.037
	0.08	0.138	0.073

4. Results and discussion

Fig. 3 shows the effects of suspension and air velocities on the pseudo-steady filtration flux. The experiments are repeated at least

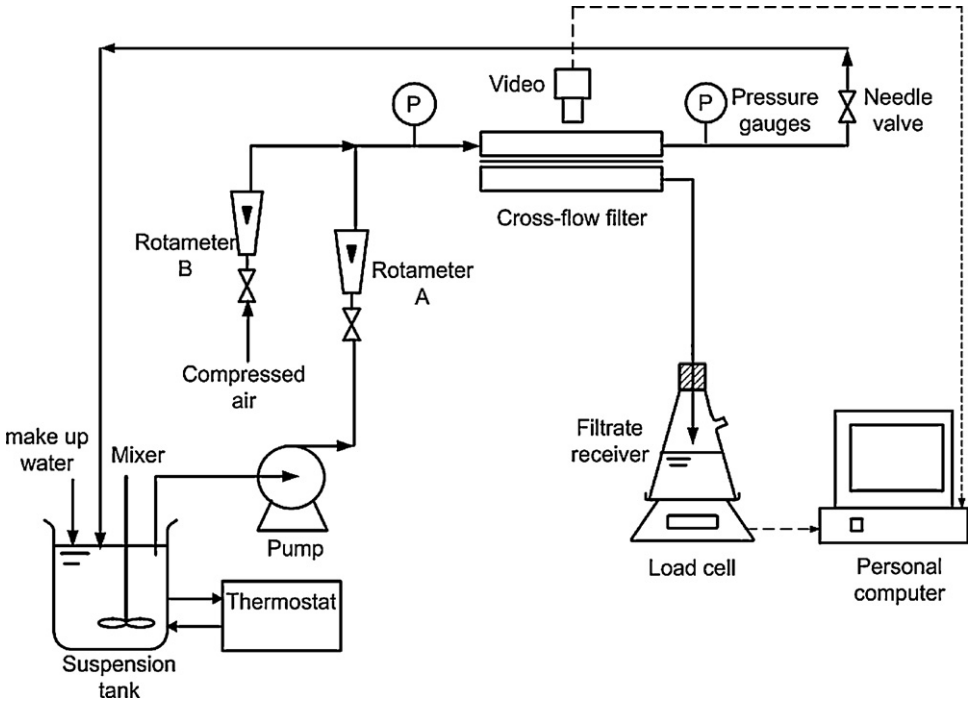

Fig. 2. A schematic diagram of cross-flow microfiltration system.

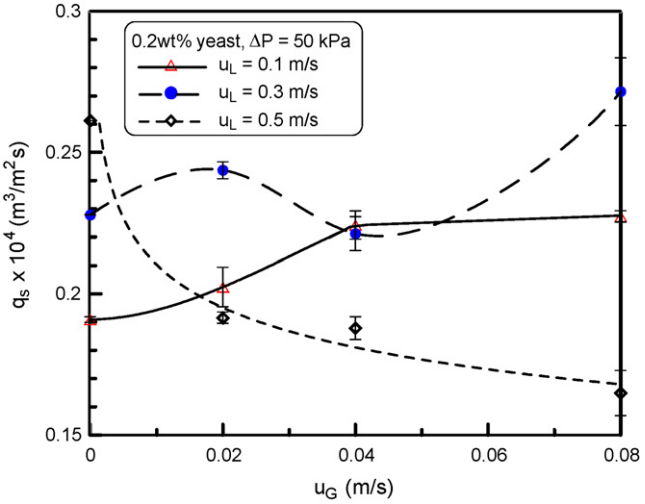

Fig. 3. The pseudo-steady filtration fluxes under various operating conditions.

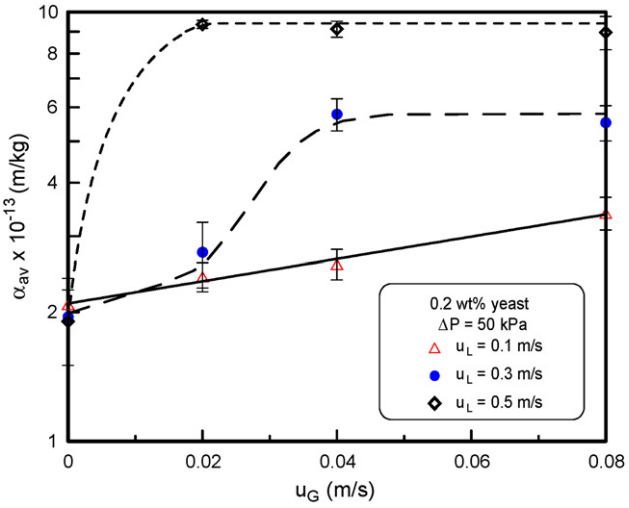

Fig. 5. Effects of operating conditions on the average specific filtration resistance of cake.

three times for each condition. The error bars shown in this figure indicate that the largest deviation on filtration flux is *ca* 15%. In the conditions of no air-sparging, the flux increases regularly with increasing suspension velocity. It is because the higher wall shear stress reduces the cake formation. This trend is the same as those presented in previous studies [17]. However, irregular trends occur in those air-sparging conditions. In the cases of lowest suspension velocity, says u_L = 0.1 m/s, the flux is increased by increasing air velocity, but this effect becomes trivial when u_G exceeds 0.04 m/s. For the suspension velocity of 0.3 m/s, the flux varies irregularly with gas velocity; the flux may be increased or decreased by increasing gas velocity. For a higher suspension velocity, u_L = 0.5 m/s, on the contrary, the air-sparging causes the flux to be drastically decreased, but the decrease becomes moderate as u_G exceeds 0.02 m/s. Although most previous studies indicated that air-sparging will effectively enhance filtration flux, the experimental data of Cabassud et al. [8] showed that a maximum flux occurred at a specific air velocity. This fact implies that the cake properties may be markedly affected by air-sparging and more than one factor should be taken into consideration for the actual filtration mechanism.

Fig. 4 shows the cake masses under various flow conditions. An increase in suspension or gas velocity leads to a decrease in cake mass. Over 40% of cake mass can be reduced by air-sparging within the operating conditions of this study. The monotonic trend shown in this figure implies that the shear stress acting on the membrane surface plays the most important role on the cake formation. In other words, the decrease in cake mass is major attributed to the increase in the wall shear stress. Fewer particles can deposit stably on the membrane surface under higher wall shear stress. Comparing the curves shown in Fig. 4, in the case of low suspension velocity, e.g., u_L = 0.1 m/s, the cake mass decreases continuously with increasing gas velocity. However, for a higher suspension velocity, the decrease in cake mass may reach an ultimate value, and this limited cake mass occurs at lower gas velocity under a higher suspension velocity. This reveals that the reduction of cake mass by air-sparging has a limit. No further effectiveness can be done by increasing air velocity when the limiting conditions attain. Therefore, on the economic point of view, to understand how the cake mass or filtration flux affected by operating conditions is very important.

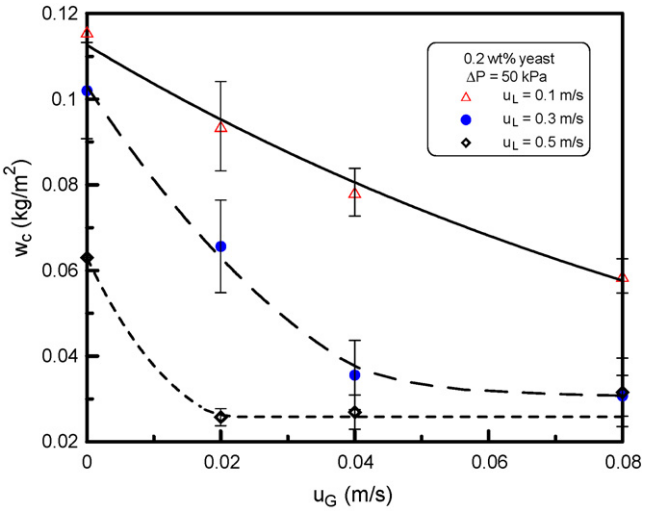

Fig. 4. Effects of operating conditions on the cake mass.

Another important cake property is the average specific filtration resistance of cake, α_{av}. The values of α_{av} under various flow conditions are shown in Fig. 5. Those values are calculated by substituting measured data of overall filtration resistance and cake mass into Eq. (12). In the conditions of no air-sparging, no obvious difference among the results of three different suspension velocities can be seen. However, when air bubbles are sparged into the filter channel, the packed structure of particles becomes more compact, and the specific filtration resistance of cake increases [12]. The increase in α_{av} becomes more significant as suspension velocity increases. However, the same as cake mass, α_{av} approaches an ultimate value when air velocity exceeds a certain value. An increase in suspension velocity leads to a higher ultimate α_{av} and to a lower critical air velocity reaching the ultimate α_{av}. It can be found that the value of α_{av} may be increased as high as five-fold due to air-sparging.

Fig. 6 depicts the structures of cakes constructed from yeast cells measured by SEM under u_L = 0.1 m/s and ΔP = 50 kPa. Fig. 6(a) and (b) shows the side views of the cakes formed under u_G = 0 and 0.02 m/s, respectively. It is evident that the cake will be compressed to a more compact structure due to air-sparging. The yeast cells almost keep their original shape, i.e. spheroid, in the cake formed under the condition of no air-sparging, while those in the cake under the air-sparging condition may deform their shape and be packed into more compact structure. This is because the flowing bubbles through the narrow filter channel exert extra compression forces on the deposited yeast cells. Consequently, those cakes

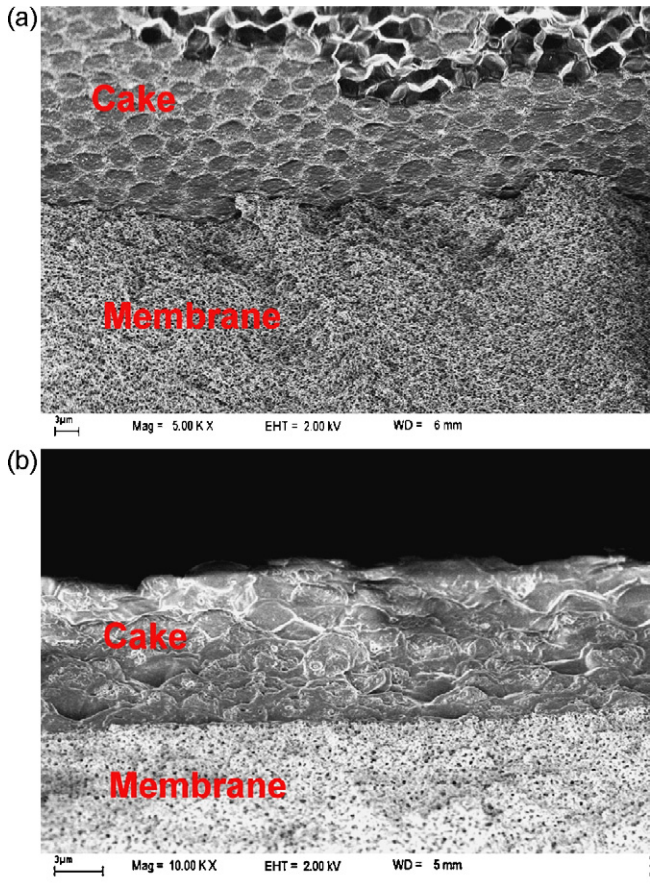

Fig. 6. The side views of particle packing structure under $u_L = 0.1$ m/s and $\Delta P = 50$ kPa: (a) $u_G = 0$ (SEM 5000×); (b) $u_G = 0.02$ m/s (SEM 10,000×).

formed under air-sparging conditions will exhibit higher average specific filtration resistances, as shown in Fig. 5.

The flows of gas and liquid phases are both laminar within the operating conditions of this study since the Reynolds numbers are smaller than 1000. The void fraction, λ, of the multiphase flow under various conditions are calculated by the two-phase flow model [12] and listed in Table 1. The values of λ are all set to be smaller than 0.3 in this study. Since the flow pattern of air bubbles is one of the key factors affecting the filtration flux as well as the cake properties. The images of flowing air bubbles under various conditions were captured by a video camera and are re-plotted in Fig. 7 for comparison. Fig. 7(a), on the left-hand side, shows the gas–liquid flow patterns under $u_L = 0.1$ m/s. In the case of $u_G = 0.02$ m/s, the flow pattern is bubbly/slug flow, and it becomes slug flows as u_G is higher than 0.04 m/s. This is in fit with the results of Cabassud et al. [8], the flow pattern changes from bubbly to slug flow when the injection factor, θ, exceeds 0.2. On the other hand, Fig. 7(b) shows the flow patterns under $u_L = 0.5$ m/s. From the data shown in Table 1, the values of θ in those conditions are all smaller than 0.2 and results in bubbly flows. Based on the analyses previously, the shear stress can be calculated by the gas–liquid two-phase flow model, Eq. (2), for a bubbly flow, while calculated by Eq. (4) for a slug flow. It can be expected that the wall shear stress increases with increasing both suspension and air velocities due to the increase in size and frequency of injecting bubbles, as shown in Fig. 7. However, the increase of wall shear stress by increasing air velocity for slug flows will be more significant than that for bubbly flows based on the proposed theories.

Fig. 8 illustrates the relationship between cake mass and the shear stress acting on the membrane surface under various operating conditions. The shear stress is calculated by Eq. (2) or (4) depending on the flow patterns, while the cake mass is measured at the end of filtration. Each kind of symbols in the figure represents the results obtained under a fixed suspension velocity. Although most filtration pressures are set at 50 kPa, a set of data obtained under different filtration pressure, $\Delta P = 75$ kPa, are also shown as

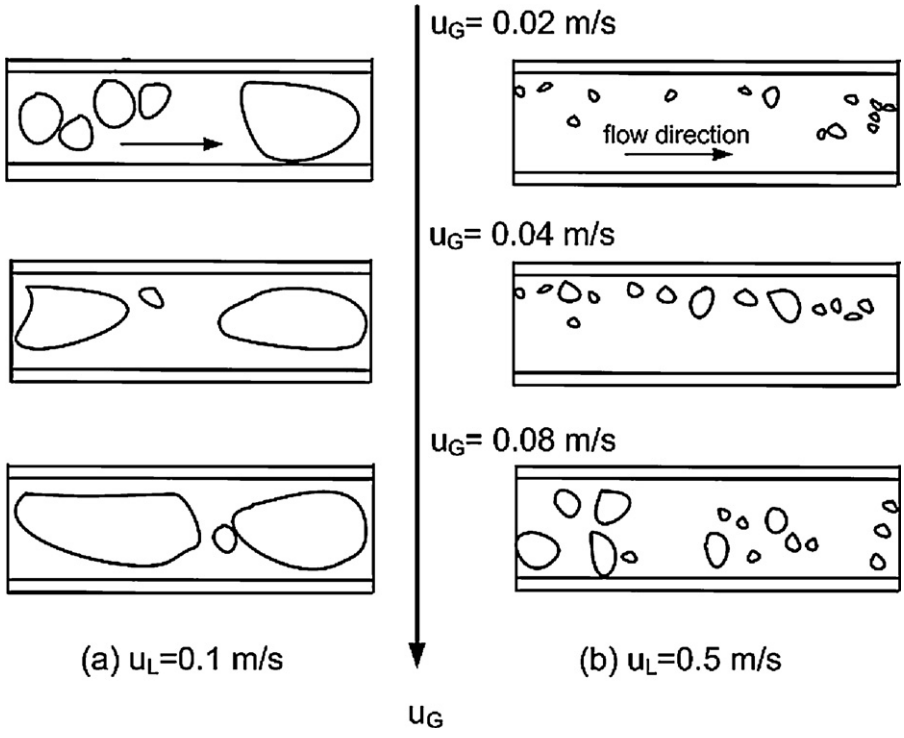

Fig. 7. The gas–liquid flow patterns under various air superficial velocities: (a) $u_L = 0.1$ m/s; (b) $u_L = 0.5$ m/s.

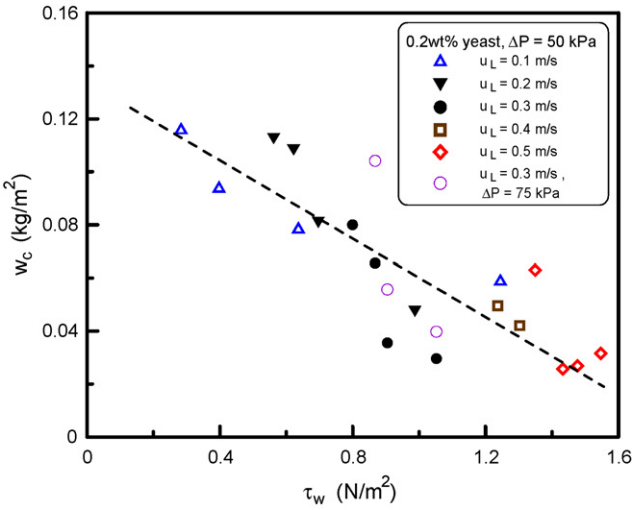

Fig. 8. Effect of wall shear stress on the cake mass.

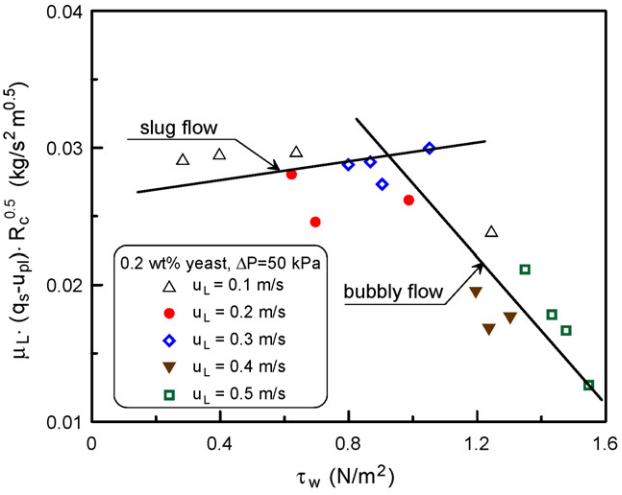

Fig. 10. A plot of $\mu_L(q_s - u_{pl})R_c^{0.5}$ versus τ_w.

hollow circles for comparison. It can be seen that the cake mass almost linearly decreases with the increase of wall shear stress. This can be expected since an increase in wall shear stress causes yeast cells to be harder to deposit on the membrane surface, as those discussions for Fig. 4. The results shown in Fig. 8 also demonstrate that the wall shear stress is the key factor affecting cake formation.

Since the filtration flux shows an irregular trend with operating conditions in Fig. 3, the cake mass should not be the sole factor in determining the overall filtration resistance. Fig. 9 depicts the average specific filtration resistance of cake under various wall shear stresses. The increase of α_{av} with τ_w implies that the cake structure is more compact under a higher tangential shear stress. The data shown in this figure can be concluded into two groups depending on the gas–liquid flow pattern, i.e., the values of α_{av} can be regressed as exponential functions as following:

$$\alpha_{av} = 1.85 \times 10^{13} \exp(0.47\tau_w) \quad \ldots \text{slug flow} \tag{18}$$

$$\alpha_{av} = 1.85 \times 10^{13} \exp(1.04\tau_w) \quad \ldots \text{bubbly flow} \tag{19}$$

Extrapolating these functions to $\tau_w = 0$, they give the same intercept at which $\alpha_{av} = 1.85 \times 10^{13}$ m/kg. This value agrees with the experimental data obtained in a "dead-end" cake filtration under $\Delta P = 50$ kPa. These results reveal that the cake structure is significantly affected by gas–liquid flow pattern. For example, the cake formed in a bubbly flow is more compact than that formed in a slug flow even under the same shear stress because of the smaller bubble size and higher bubble frequency. Therefore, for the curves shown in Fig. 5, one knows that the sudden increase in α_{av} at a certain air velocity is due to the flow pattern change. According to Eq. (12), the filtration resistance can be expressed as the product of cake mass and average specific filtration resistance of cake. The results shown in Figs. 8 and 9 indicate that cake mass monotonically decreases while average specific filtration resistance of cake increases with the wall shear stress. These two contrary effects result in the irregular trends of overall filtration resistance and filtration flux under different flow conditions, as shown in Fig. 3. Thus, how filtration flux affected by operating conditions can be well understood only when these two cake properties are taken into consideration simultaneously. Concluding the results obtained in the conditions of this study, the flux may be enhanced by air-sparging due to the cake reduction in slug flow microfiltration. However, contrary result may be obtained for bubbly flow due to the increase of average specific filtration resistance of cake.

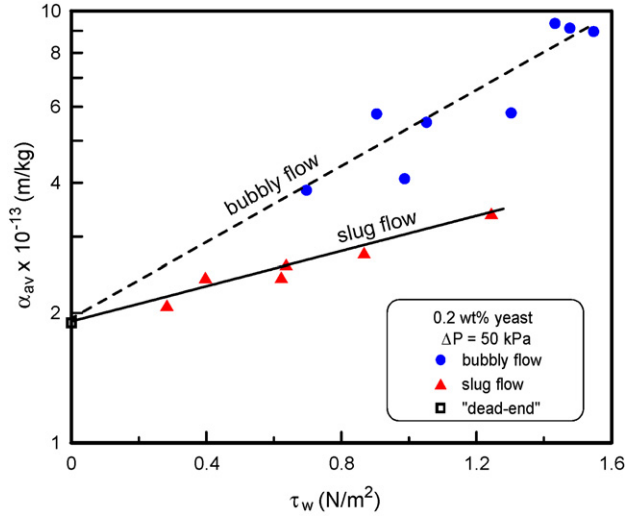

Fig. 9. Effect of wall shear stress on the average specific filtration resistance of cake.

Based on the proposed force balance model for particle deposition, the relationship among the pseudo-steady filtration flux, the wall shear stress and the overall filtration resistance can be correlated by Eq. (16). This equation reveals a linear relationship between $\mu_L(q_s - u_{pl})R_c^{0.5}$ and τ_w if the membrane resistance can be neglected compared to the cake resistance. Fig. 10 shows a plot of $\mu_L(q_s - u_{pl})R_c^{0.5}$ versus τ_w under a constant filtration pressure of 50 kPa. The data obtained under different conditions can be regressed to two line segments. The value of $\mu_L(q_s - u_{pl})R_c^{0.5}$ increases linearly with the wall shear stress for slug flows; however, it decreases with τ_w for bubbly flows. This difference is attributed to the effect of flow pattern on the cake properties. Since the particle packing structure or the average specific filtration resistance of cake is strongly affected by the gas–liquid flow pattern even under the same wall shear stress, no wonder the regression lines for bubbly and slug flows shown in Fig. 10 are different. The results shown in Figs. 3 and 10 also indicates that increasing shear stress is more effective for flux enhancement in slug flows, but contrary effect occurs in bubbly flows. However, the plot in Fig. 10 can be regressed to straight lines according to the flow patterns. This demonstrates the reliability and practicability of the proposed force balance model. In other words, the filtration flux can be predicted by solving Eq. (16) once the properties of particles and cake are known.

5. Conclusion

The influence of air-sparging on the performance of cross-flow microfiltration of yeast suspension has been studied. The filtration performance is affected by the gas–liquid flow pattern (or the wall shear stress) rather than fluid velocities. The shear stress acting on the membrane surface was analyzed based on hydrodynamic models. The cake mass was significantly reduced by increasing the wall shear stress, while the average specific cake filtration resistance increased with increasing the wall shear stress due to more compact cake structure. The increase in specific filtration resistance of cake due to air-sparging was more significant in bubbly flows. Consequently, the filtration flux was increased by air-sparging due to cake reduction for slug flow microfiltration under the conditions of this study. However, a contrary result was obtained for bubbly flows due to the drastic increase in the average specific filtration resistance of cake. To operate the filtration in slug flow pattern was more effective on the viewpoint of flux enhancement. Furthermore, the filtration flux was related to operating parameters based on the proposed force balance model. The relationships were also strongly dependent on the gas–liquid flow pattern.

Acknowledgement

The authors wish to express their sincere gratitude to the National Science Council of the Republic of China for its financial support.

References

[1] Z.F. Cui, K.I.T. Wright, Gas–liquid two phase flow ultrafiltration of BSA and dextran solutions, J. Membr. Sci. 90 (1994) 183–189.
[2] Z.F. Cui, K.I.T. Wright, Flux enhancements with gas sparging in downwards crossflow ultrafiltration: performances and mechanisms, J. Membr. Sci. 117 (1996) 109–116.
[3] M. Mercier-Bonin, C. Lagane, C. Fonade, Influence of a gas/liquid two-phase flow on the ultrafiltration and microfiltration performances: case of a ceramic flat sheet membrane, J. Membr. Sci. 180 (2000) 93–102.
[4] M. Mercier-Bonin, C. Fonade, Air-sparged microfiltration of enzyme/yeast mixtures: determination of optimal conditions for enzyme recovery, Desalination 148 (2002) 171–176.
[5] P. Mikulášek, P. Pospišil, P. Dolecek, J. Cakl, Gas–liquid two-phase flow in microfiltration mineral tubular membranes: relationship between flux enhancement and hydrodynamic parameters, Desalination 146 (2002) 103–109.
[6] P. Pospišil, R.J. Wakeman, I.O.A. Hodgson, P. Mikulášek, Shear stress-based modelling of steady state permeate flux in microfiltration enhanced by two-phase flows, Chem. Eng. J. 97 (2004) 257–263.
[7] C.K. Lee, W.G. Chang, Y.H. Ju, Air slugs entrapped cross-flow filtration of bacterial suspensions, Biotechnol. Bioeng. 41 (1993) 525–530.
[8] C. Cabassud, S. Laborie, L. Durand-Bourlier, J.M. Lainé, Air sparging in ultrafiltration hollow fibers: relationship between flux enhancement, cake characteristics and hydrodynamic parameters, J. Membr. Sci. 181 (2001) 57–69.
[9] S. Chang, A.G. Fane, Filtration of biomass with axial inter-fibre upward slug flow: performance and mechanisms, J. Membr. Sci. 180 (2000) 57–68.
[10] A.G. Fane, S. Chang, E. Chardon, Submerged hollow fibre membrane module-design options and operational considerations, Desalination 146 (2002) 231–236.
[11] A.P.S. Yeo, A.W.K. Law, A.G. Fane, The relationship between performance of submerged hollow fibers and bubble-induced phenomena examined by particle image velocimetry, J. Membr. Sci. 304 (2007) 125–137.
[12] K.J. Hwang, Y.J. Wu, Flux enhancement and cake formation in air-sparged cross-flow microfiltration, Chem. Eng. J. 139 (2008) 296–303.
[13] J.O. Wilkes, Fluid Mechanics for Chemical Engineers, Chap.10, Prentice Hall, New Jersey, USA, 2006, pp. 468–474.
[14] M. Mercier-Bonin, G. Gésan-Guiziou, C. Fonade, Application of gas/liquid two-phase flows during crossflow microfiltration of skimmed milk under constant transmembrane pressure conditions, J. Membr. Sci. 218 (2003) 93–105.
[15] M.I. Briceño, D.D. Joseph, Self-lubricated transport of aqueous foams in horizontal conduits, Int. J. Multiphase Flow 29 (2003) 1817–1831.
[16] F.P. Bretherton, The motion of long bubbles in tubes, J. Fluid Mech. 10 (1961) 166–188.
[17] W.M. Lu, K.J. Hwang, Cake formation in 2-D cross-flow filtration, AIChEJ 41 (6) (1995) 1443–1455.
[18] K.J. Hwang, K.P. Lin, Cross-flow microfiltration of dual-sized submicron particles, Sep. Sci. Technol. 37 (2002) 2231–2249.
[19] S.L. Goren, The hydrodynamic force resisting the approach of a sphere to a plane permeable wall, J. Colloid Interface Sci. 69 (1979) 78–85.
[20] D.A. Drew, J.A. Schonberg, G. Belfort, Lateral inertial migration of a small sphere in fast laminar flow through a membrane duct, Chem. Eng. Sci. 46 (1991) 3219–3224.
[21] K.R. Tsang, P.A. Vesilind, Moisture distribution in sludge, Water Sci. Technol. 22 (1990) 135–142.